heritage

MDPI

Article

Study of an Iron Age Gilded Silver Earring by XRF, SEM-EDS and Multifocus OM

Sofia Serrano [1,*], Alexandra Rodrigues [2], Rui J. C. Silva [1] and Elin Figueiredo [1,*]

1 Centro de Investigação de Materiais (CENIMAT/i3N), School of Science and Technology, NOVA University of Lisbon, Campus de Caparica, 2829-516 Caparica, Portugal
2 Vidro e Cerâmica para as Artes (VICARTE), School of Science and Technology, NOVA University of Lisbon, Campus de Caparica, 2829-516 Caparica, Portugal
* Correspondence: spe.serrano@campus.fct.unl.pt (S.S.); esf@fct.unl.pt (E.F.)

Abstract: The use of gold for artefact productions underwent substantial developments during Iron Age in western Europe, with the diversification of alloy compositions and the introduction of new technologies and aesthetics. This work presents a detailed study of a Late Iron Age earring from the western Iberian Peninsula and a discussion taking into consideration the alloys and technologies used at the time. The earring has a complex structure, composed of block- and strip-twisted wires and granulation. Characterization by multifocus optical microscopy, portable X-ray fluorescence spectrometry (pXRF), micro-XRF and scanning electron microscopy with energy dispersive spectroscopy (SEM-EDS) were performed to obtain information on the chemical composition and manufacturing techniques. Results show that the earring was manufactured with wires and granules made of a silver-rich alloy, covered with a gold-rich layer 45 μm thick on average, which acted as an external coating making the entire earring resemble gold. This is a rare example of an Iron Age gilded earring, and its detailed study provides further information on the manufacturing solutions adopted by the Iron Age goldsmiths.

**Keywords:** gilding; gold; silver; iron age; iberian peninsula; archaeometallurgy

1. Introduction

Gold began to be used in the Iberian Peninsula during the Chalcolithic period (c. 4000–2000 BCE) to produce relatively simple objects with decorative functions [1,2]. During the Bronze Age (BA) (c. 2000–800 BCE) more complex modelling and joining techniques began to be used, like lost-wax casting and casting-on techniques [3–5], which resulted in the production of large and massive objects. During this period, artefacts such as necklaces, bracelets, diadems, earrings and torcs were frequently massive and decorated with geometric motifs on the surface, usually made with a chisel and a punch [3,6,7]. By Late Bronze Age (LBA) (c. 1200–800 BCE), chiselling and polishing techniques were a common practice for surface finishing and decoration [2].

During BA, the alloy composition of the artefacts was mainly related to the composition of the native gold that was used, which varied according to the gold source [8,9]. In western Iberia, native gold sources could be found in the form of small nuggets in alluvial deposits, which would be collected and melted together to produce an artefact [2]. This native gold usually contains 5 to 25 wt.% Ag [10], being this compositional range usual in the BA gold artefacts. Although copper is normally not part of native gold, it can be found in the artefact alloys in low contents, usually <1 wt.% [10,11], and can be understood as a contamination that happened during metallurgical practices, as from copper and bronze metallurgy, which were the most usual metals at the time.

During the Iron Age (IA) (c. 800 – 100 BCE), significant changes occurred in western Iberia. During this period, an intensification of contacts with cultures from the eastern Mediterranean happened and resulted in the incorporation of new aesthetic tastes and

technological solutions. Plastic-shaping techniques became recurrent, such as filigree and granulation, and soldering or brazing was used to join different elements [8,12–14]. During this period the composition of the alloys began to diversify, with the introduction of Au-Ag-Cu intentional alloys and refining techniques [12,15,16]. Although resulting in a large variability of compositions, one of the main differences compared to the previous period (BA) was a general increase in Ag and Cu contents in the alloys, with alloys showing >20 wt.% Ag, and 2 to 10 wt.% Cu [1,14,17–21]. An increase of Ag and Cu in the gold has repercussions in the *liquidus* temperature of the alloy. For instance, when changing from an alloy with 10 wt.% Ag to an alloy with 40 wt.% Ag and 20 wt.% Cu a decrease of 150 °C in the *liquidus* temperature (from ca. 1050 to 900 °C) happens. Also, considering the previous example, a change in colour, from yellow to pale greenish yellow occurs [5,22,23] (Figure 1). Furthermore, the use of alloys with higher amounts of Ag and Cu can be understood as being more "economic" [12,15,24].

(**a**)

(**b**)
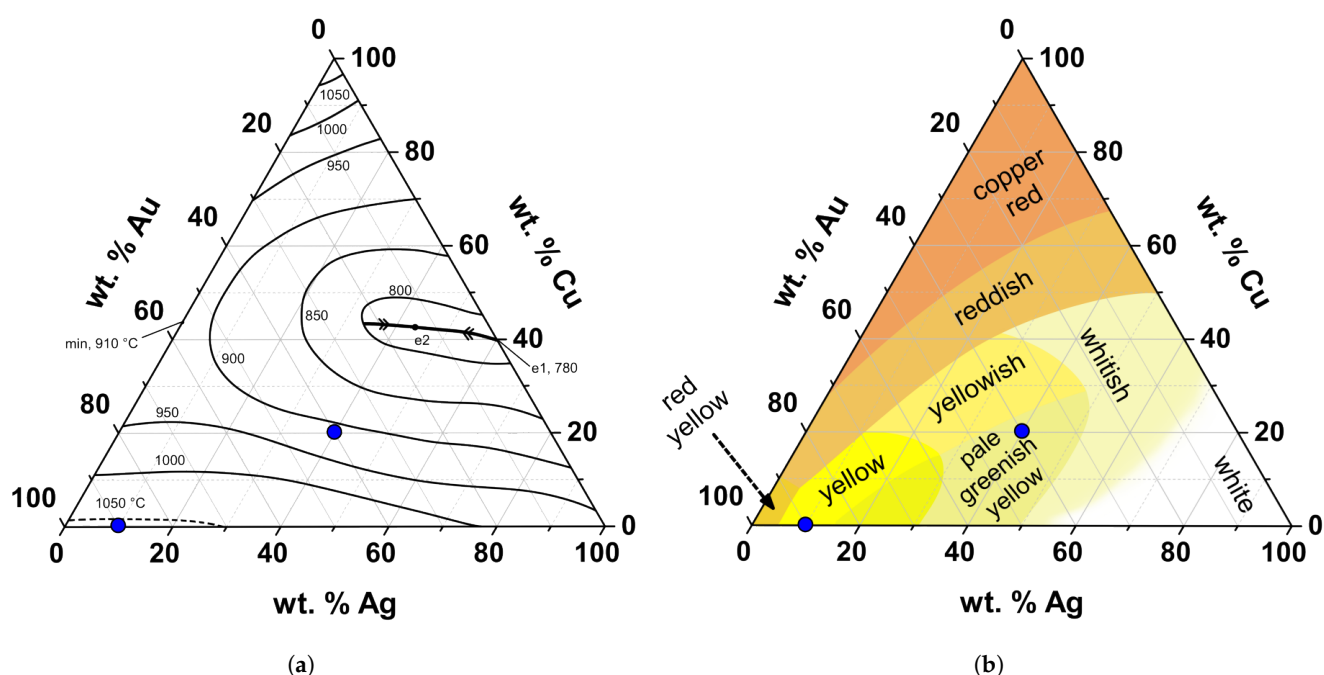
Figure 1. Ternary diagrams of the Au-Ag-Cu alloy showing (**a**) the phase diagram (adapted and redesigned from [23]) and (**b**) different colours obtained with different alloy compositions (adapted and redesigned from [5]). The blue dots represent two gold alloys, one with 10 wt.% Ag (yellow colour) and another with 40 wt.% Ag and 20 wt.% Cu (pale greenish yellow colour).

In the present work, an IA artefact that belongs to a private collection, most likely destined to be worn as an earring ("*arrecada*" type) (Figure 2), will be studied in detail. The earring has a c-shape body composed of six wires. The lower external surface of the earring is outlined by seven granules, of which two are missing. The top ends have a hole (one side has a missing part) that probably served to place a hanging or fastening element.

During the IA, metal wires were frequently used for decorative or structural functions. Wires could have different diameters and cross-sections and were frequently twisted to provide distinctive decorative effects. The manufacture of wires previously to the use of draw plates was based on the technique of twisting a metal strip. Two techniques could be employed: strip-twist, detected by the pattern of diagonal line depressions along the length of the wire, or block-twist, resulting in diagonal edges along the wire when finished [25–28]. For each technique, the wires could be twisted clockwise (S-twist) or counterclockwise (Z-twist). In the studied earring, the two central wires were twisted with the block-twist technique (one S-twisted and the other Z-twisted), and the remaining four wires were twisted with the strip-twist technique (three S-twisted and one Z-twisted).

Figure 2. Photograph of the IA earring under study, showing a body composed by six wires and seven granules, two of which are missing. Earring's dimensions (cm) are 2.56 × 2.26 × 0.04–0.18 (width × length × thickness) and its weight is 1.13 g.

For the present study, the earring was examined by optical microscopy to search for surface heterogeneities and analyzed by X-ray fluorescence spectrometry (XRF) and by scanning electron microscopy with Energy Dispersive Spectroscopy (SEM-EDS) for elemental heterogeneity studies. The XRF quantitative analysis considers both Ag-Lα and Ag-Kα characteristic X-rays, since L lines emerge from a smaller depth than the K lines, being possible an evaluation of composition heterogeneities along depth. Such heterogeneities can result from corrosion, such as a natural surface dissolution of the less noble elements of gold alloys [29] or be a result of the original materiality of the object.

2. Materials and Methods

2.1. Multifocus Optical Microscopy

Detailed observations of the surface of the earring were performed using a multifocus digital optical microscope (OM) Dino-Lite AM7915MZTL – EDGE, with a 5 megapixels image capture and a magnification of 10–140×. These observations allowed a better interpretation of the manufacturing techniques and altered surfaces. By using the snap mode (SM) and extended depth of field (EDOF) functionalities through the DinoCapture 2.0 software it was possible to record near-flat and non-flat surfaces, of great importance for the interpretation of metal and corroded surfaces [30]. For greater stability in capturing images, the Dino-Lite Rack (RK-10A) was used

2.2. X-ray Fluorescence Spectrometry

X-ray fluorescence spectrometry (XRF) analyses were performed with two different equipments: (i) a portable handheld equipment (pXRF) Tracer 5*i* Bruker, with a Be window and an Rh source with an area of analysis of approximately 3 mm in diameter; and (ii) a micro-XRF equipment, ArtTax (Intax GmbH; Bruker) spectrometer, with an 8 µm Be window, a Mo source, and an area of analysis smaller than 100 µm in diameter. For the pXRF analysis, a voltage of 40 kV, a current of 30 µA and an acquisition time of 100 s was used. For the micro-XRF analysis a voltage of 40 kV, current of 600 µA and an acquisition time of 100 s was used.

Qualitative analyses were carried out with the ARTAX software, and quantitative analyses were carried out with the software bAxil, which uses a fundamental parameter method and experimental calibration factors that were calculated with the following certified reference materials: Gold ERM-EB506, Gold ERM-EB507 and Gold ERM-EB508 for the pXRF analysis; Au-Ag-Cu standard IAEA I, II, III and IV for the micro-XRF analysis.

The experimental relative error for the pXRF analysis was calculated as lower than 7% for the three alloy constituents Au, Ag and Cu, and quantification limits were calculated as: 0.06 wt.% Au-L lines; 0.09 wt.% Ag-K lines; 0.11 wt.% Ag-L lines; 0.03 wt.% Cu-K lines. For the micro-XRF analysis, the experimental relative error was calculated as lower than 4% and quantification limits were calculated as: 0.03 wt.% Au-L lines; 1.30 wt.% Ag-K lines; 1.34 wt.% Ag-L lines; 0.15 wt.% Cu-K lines.

Use of Ag-L and Ag-K lines in XRF

When analyzing ancient metals, a probable lack of material homogeneity at surface areas and along depth has to be taken into consideration. Surface heterogeneities can be evaluated through analysis in different areas of an artefact. Depth heterogeneities can only be evaluated in a non-invasive way taking advantage of the use of low and higher characteristic energy lines that originate from thinner or thicker substrates, respectively.

The depth of analysis from which a percentage of fluorescent X-rays originates in gold, silver or copper matrixes were calculated for energies of interest. The depth (d) in micron from which a chosen percentage (x) of fluorescent X-rays originates is given by the following equation [31,32]:

$$d = 10,000(\ln(100/100 - x))/\mu\rho$$

where μ is the alloy (matrix) mass attenuation coefficient (cm^2/g) for the X-rays of interest and ρ is the density (g/cm^3) of the alloy. For the present calculation, a 90° angle position is considered for the detector, to obtain maximum depth values. A smaller angle will decrease the depth of analysis.

In Table 1 are the mass attenuation coefficients calculated for elements and X-rays of interest in the present work.

Table 1. Mass attenuation coefficients (cm^2/g) for particular X-ray energies (Au-Lα, Ag-Kα, Ag-Lα, Cu-Kα) considering pure (100%) gold, silver and copper matrixes [33].

		Matrix		
		Au	**Ag**	**Cu**
L alpha	Ag (2.98431 keV)	457.69	533.26	798.10
	Au (9.7133 keV)	129.06	131.45	236.39
K alpha	Cu (8.04778 keV)	207.37	217.77	51.41
	Ag (22.1629 keV)	59.92	13.56	25.42

Calculations of the depth of analysis are shown in Table 2. Considering a gold matrix, the analysis will include a subtract 60 μm thick. However, most of the radiation (90%) will originate from a <20 μm depth. Considering a silver matrix, analysis can be deeper, mostly when considering the K lines for silver that can originate from depths up to 480 μm. However, most of these lines (90%) originate from much smaller depths, <160 μm.

When taking into account a gold or silver matrix, the depth of analysis considering specific X-ray lines will decrease in the following order: Ag-Kα> Au-Lα> Cu-Kα>Ag-Lα. Thus, if surface composition heterogeneities are to be detected in the present work, Ag-K and Ag-L lines shall be used separately for quantification, since Ag-K lines derives from much greater depths than Ag-L (7 × deeper in Au matrix and 40 × deeper in Ag matrix).

Table 2. Calculation of the depth in microns from which a chosen percentage of fluorescent X-rays originates when considering a gold matrix (density of 19.37 g/cm³), a silver matrix (density of 10.50 g/cm³) and a copper matrix (density of 8.94 g/cm³).

		Percentage of Fluorescent X-Rays			
		20%	**50%**	**90%**	**99.9%**
Au matrix	Ag-Lα	0.3	0.8	2.6	7.8
	Au-Lα	0.9	2.8	9.2	27.6
	Cu-Kα	0.6	1.7	5.7	17.2
	Ag-Kα	1.9	6.0	19.8	59.5
Ag matrix	Ag-Lα	0.4	1.2	4.1	12.3
	Au-Lα	1.6	5.0	16.7	50.0
	Cu-Kα	1.0	3.0	10.1	30.2
	Ag-Kα	15.7	48.7	161.7	485.2
Cu matrix	Ag-Lα	0.3	1.0	3.2	9.7
	Au-Lα	1.1	3.3	10.9	32.7
	Cu-Kα	4.9	15.1	50.1	150.3
	Ag-Kα	9.8	30.5	101.3	304.0

2.3. Scanning Electron Microscopy with Energy Dispersive Spectroscopy

The scanning electron microscopy (SEM) analysis was carried out in a Zeiss DSM 962 equipment, with secondary electrons (SE), backscattered electrons (BSE) and an energy dispersive spectroscopy (EDS) detector (Oxford INCAx-act LN2-free Analytical 10 mm², resolution of 125 eV at Mn-K, 5.9 keV,). The experimental conditions involved a working distance of 25 mm, an acceleration voltage of 20 kV, a filament current of 3 A, and an emission current of 70 μm. The analyses were performed without any superficial conductive coating.

Regarding the SEM-EDS analysis, characteristics X-rays are emitted due to an electron bombardment, providing information of spot areas usually with 1 μm diameter and 1 μm depth (under normal operating conditions and not very light average atomic weight material) [34]. This means that regarding any characteristic X-rays of Au, Ag or Cu, the SEM-EDS analyses will always be representative of a less deep analysis than the XRF.

2.4. Surface Preparation

A small surface grinding and polishing was performed in two side areas of the earring: one (1) in the outline of the exterior wire (~2.8 × 0.4 mm) and another (2) over a missing granule (~0.4 × 0.8 mm). The grinding was made using two sandpaper with two different granulometry (P2500 and P4000). After that, a polishment with diamond paste with a granulometry of 1 μm in a cotton swab was performed and the surfaces were cleaned with ethanol. These surface preparations allowed to reach a greater depth of material, with a minimum invasive procedure. In the case of the area (1) it allowed to reach deeper material in a wire. In the case of the area (2) it allowed to analyse the region of fracture of a missing granule. These two areas were observed and analysed by OM, micro-XRF and SEM-EDS.

3. Results and Discussion

The OM observation of the earring revealed that the body of the earring is composed of six wires, mechanically joined at the top ends by compression. Observations of the granules revealed that they were composed of a core material of a dark colour, different from the outside material, which looks like a gold coating. The material that makes the bulk of the granule (core) seems to be rather poorly aggregated when compared to the gold covering material. In other areas of the earring, it is apparent small detachments of this gold coating, allowing to observe a core of darker colour material (Figure 3).

(**a**) (**b**)
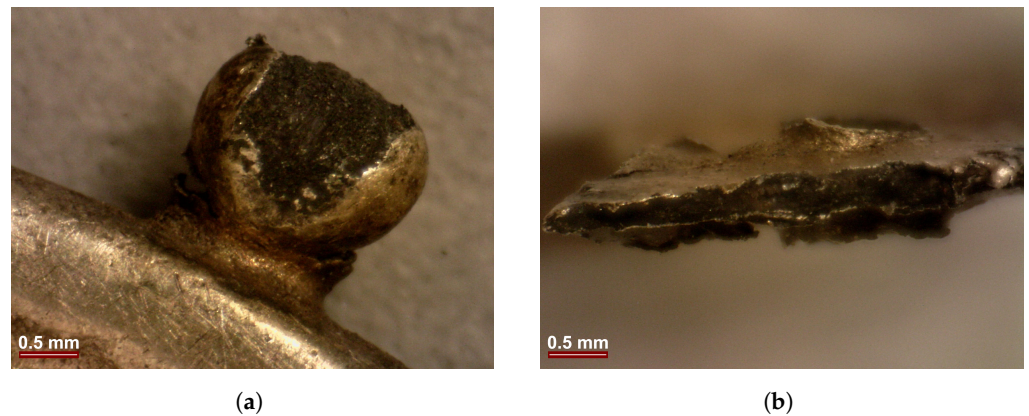
Figure 3. OM images of details of the earring: (**a**) granule of dark colour with gold coating; (**b**) top fracture of the earring showing a dark material core covered with the gold coating.

Observation by OM allowed measurements of the thickness of this gold-like coating to be made. The thickness of the coating was measured as between 25 and 85 μm, with an average of 45 μm (Figure 4).
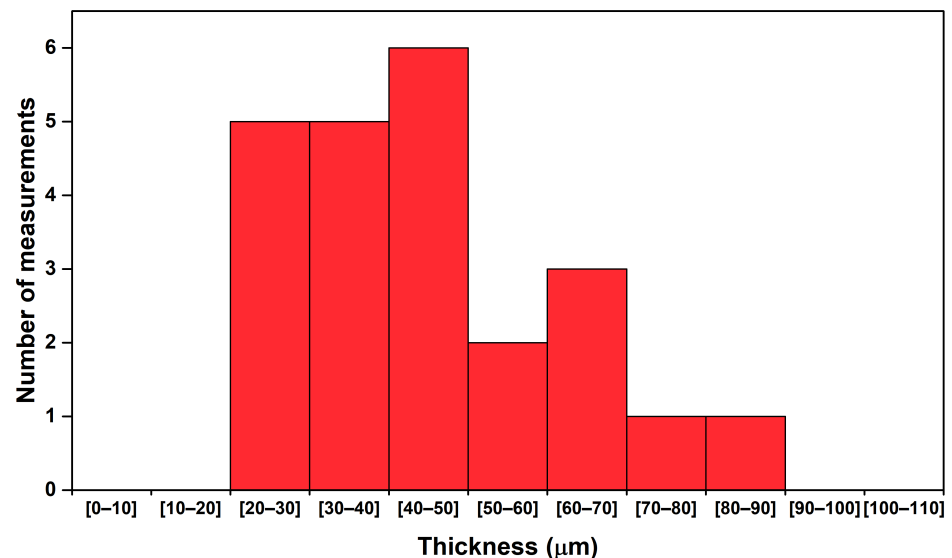

Figure 4. Measurements made by OM of the thickness of the gold coating in different areas of the earring.

pXRF analyses were carried out in three different areas of the earring to provide an estimation of the overall composition of the artefact and to account for any composition heterogeneity between areas. The results showed a fairly homogeneous composition, with a low standard deviation between the analysed areas (<2%). Results show a gold alloy with 25–30 wt.% Ag and about 8 wt.% Cu (Table 3). If considered only by themselves, the results could be interpreted as being relative to the bulk composition of the earring, which would be within the range of compositions obtained for other IA gold alloys from western Iberia (Figure 5). Considering the values obtained for Ag when using the K or L lines, these show differences of ca. 5 wt.% in all three analyses, with lower values towards the surface of the artefact (using L lines). This difference could be interpreted as a result of corrosion, due to the dissolution of the anodic constituents at the surface of the object. However, further detailed analysis allows the interpretation of these results as something else.

Table 3. Elemental composition of the earring obtained by pXRF, using different Ag lines for the quantification (average values with standard deviation, normalised to 100 wt.%).

	Au	Ag	Cu
Using Ag-K lines	61.47 ± 1.22	30.57 ± 1.86	7.98 ± 0.72
Using Ag-L lines	66.67 ± 0.45	24.80 ± 1.18	8.51 ± 0.72

• IA gold artefacts from western Iberia
• pXRF elemental composition using Ag-K lines
○ pXRF elemental composition using Ag-L lines
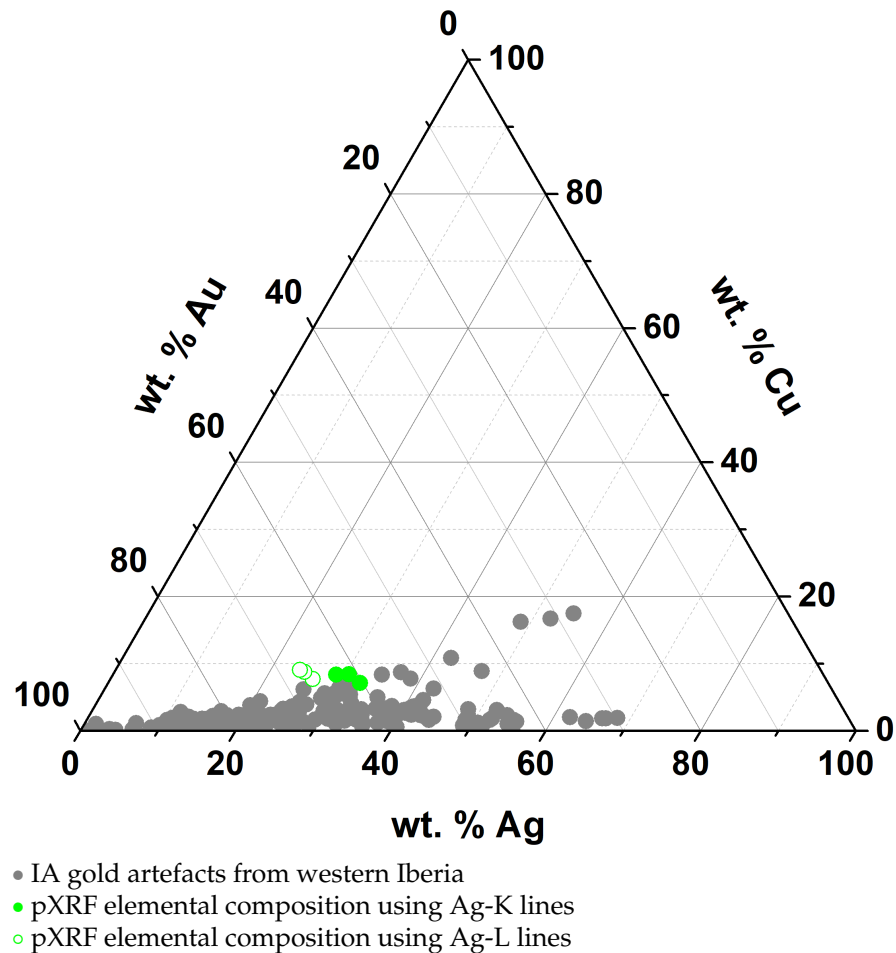
Figure 5. Elemental composition of IA gold artefacts from western Iberia based on published data [1,14,17–21] and composition of the studied earring based on pXRF analysis.

Micro-XRF analyses were performed in various spots of the earring to evaluate the heterogeneities observed by the OM. Analyses were made in the granules (material of dark colour) and over the coating. The analysis revealed that the dark colour granules are mainly composed of Ag, with only 8-13 wt.% of Au, in opposition to the coating, which has much higher Au contents, up to 66 wt.% Au. These analyses reveal that the core of the granules must have been made in a silver-rich alloy, now corroded, which was covered by a gold-rich layer, now partially missing (Figure 6). It should be noted that the analyses carried out on the dark granules revealed the presence of Cl, which can be associated with the degradation of Ag (silver chlorides).
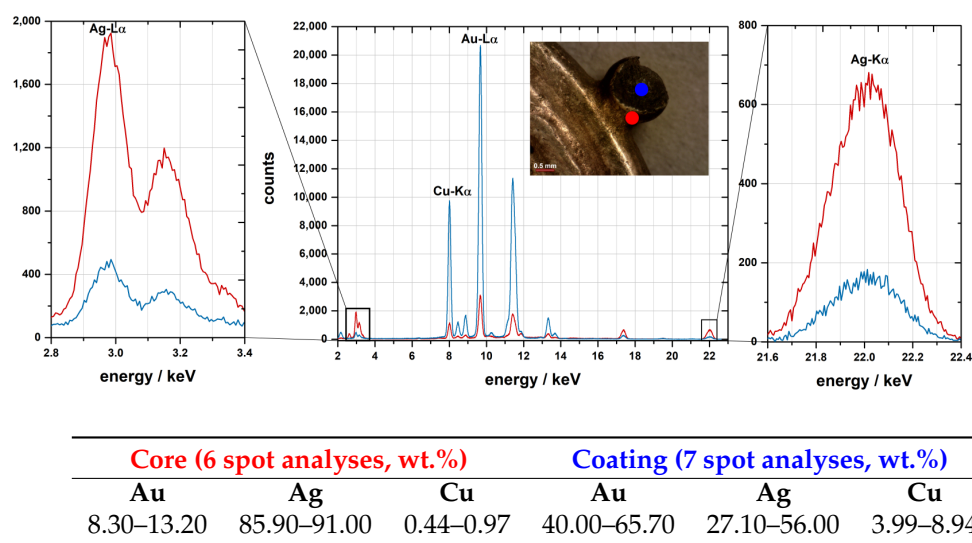
Figure 6. Micro-XRF spectra of the core and coating of a granule in the earring, with the quantitative results at the bottom (6 and 7 spot analysis in each area, quantification used Ag-L lines to avoid the influence of core composition in the coating analysis).

| Core (6 spot analyses, wt.%)			Coating (7 spot analyses, wt.%)		
Au	**Ag**	**Cu**	**Au**	**Ag**	**Cu**
8.30–13.20	85.90–91.00	0.44–0.97	40.00–65.70	27.10–56.00	3.99–8.94

Micro-XRF analyses were also made over the body of the earring to investigate if the wires, i.e., the core of the earring, could also have been made of a silver-rich alloy covered by a gold-rich layer. Numerous spot analyses were made on the diagonal edges of the wires and in the depressions between the wires, based on the hypothesis that depending on the gilding technique and the wear of the object, the thickness of the coating might not be constant throughout the artefact: likely, the coating will be thinner over the edges and thicker between the wires. The results show that in most of the analyses made on the edges of the wires an increase in the Ag values happen when compared to the areas between the wires (Figure 7). On contrary, it was observed a decrease in the Cu content in the analysis made on the edge of the wires and an increase in Cu in the areas between the wires. This Cu tendency does not follow what would be expected in the presence of a corrosion phenomenon, with the depletion of the less noble elements. If that would be the case, Cu would have decreased simultaneously to Ag, i.e., when Au contents were higher. Instead, these results demonstrate that Cu is directly related to Au and can thus be interpreted as taking part of the composition of the gold-rich layer rather than of a silver-rich core. It was also possible to observe that for most analyses, the content of Ag is higher when considering the Ag-K lines in comparison to the Ag-L lines, in agreement with the results obtained by pXRF.

In order to evaluate in greater detail the coating and the wires, the small surface prepared (area 1) was first analysed by micro-XRF with spot analysis made from the surface of the earring towards the central part of the prepared area. The central part of the prepared area corresponds to the deepest region of the wires analysed in this study. The results showed that at the centre of the prepared area Ag increased significantly, up to 75 wt.% Ag, in opposition to adjacent areas, which were Au and Cu-richer (Figure 8). This analysis shows, without any doubt, that the wires were originally made in an Ag-rich alloy, whose original composition is not known through the present analysis since the centre of the prepared area might not be representative of the most internal silver alloy (Au and Cu might continue to diminish at greater depths). On the other hand, a clear positive correlation between Cu and Au (instead of Ag) was observed by numerous micro-XRF analyses made over the prepared surface (1) (Figure 9). This association of Cu to Au, points out to the use of an Au-rich alloy with significant Cu content (when compared to the original Ag core alloy) in the coating, and thus to perform the gilding of the object. The same prepared surface was also analysed by SEM-EDS. An elemental line scan revealed a gradual Ag enrichment
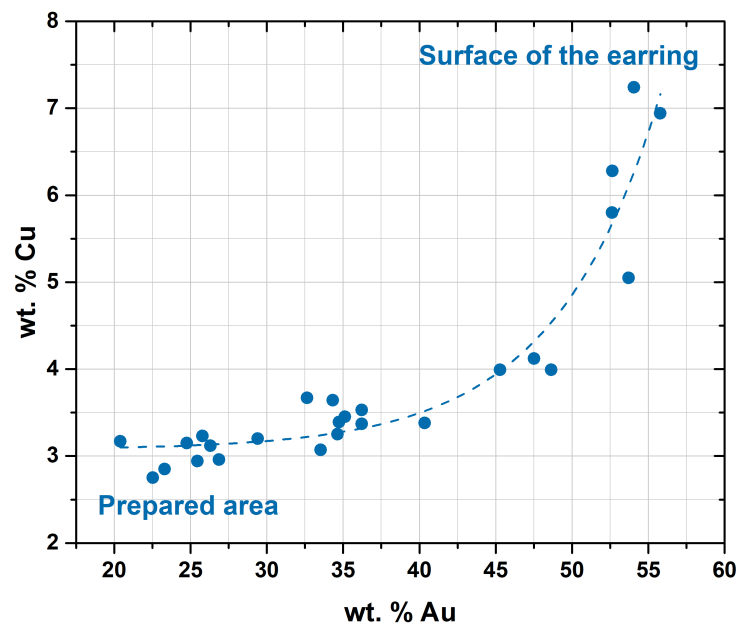
towards the centre of the prepared surface, as well as an Au and Cu decrease, proving that the artefact has an interior in a silver-rich alloy and a coating in a gold-copper-rich alloy (Figure 10). This result agrees with those made over the wires and between wires and excludes the possibility of a gilding technique performed by the dissolution of the anodic constituents at the earring's surface. Also, the absence of Hg in all the analyses (pXRF, micro-XRF and SEM-EDS) indicates that the gilding was not obtained by the technique of mercury gilding [35], which has been a technique previously identified for the gilding of silver parts in torques, from the Late Iron Age (LIA) in northern Iberia [20]. Previous published data on mercury gilded artefacts (using XRF, SEM-EDS and PIXE) [20,36,37] found Hg contents between 2 and 20 wt.%, which would have been easily detected in the present study. Other gilding processes identified in Proto-historic objects from western Iberia have included foil gilding of a bronze artefact [38] and interdiffusion gilding of a copper artefact [16]. Given the compositional gradient observed from the surface of the earring towards the centre of the prepared area (1), a gilding involving a diffusion process seems the most probable in the case of this earring.

□ Wires (**W**) | ● Between wires (**B**) | ● Au | ● Ag-L lines | ● Ag-K lines) | ● Cu
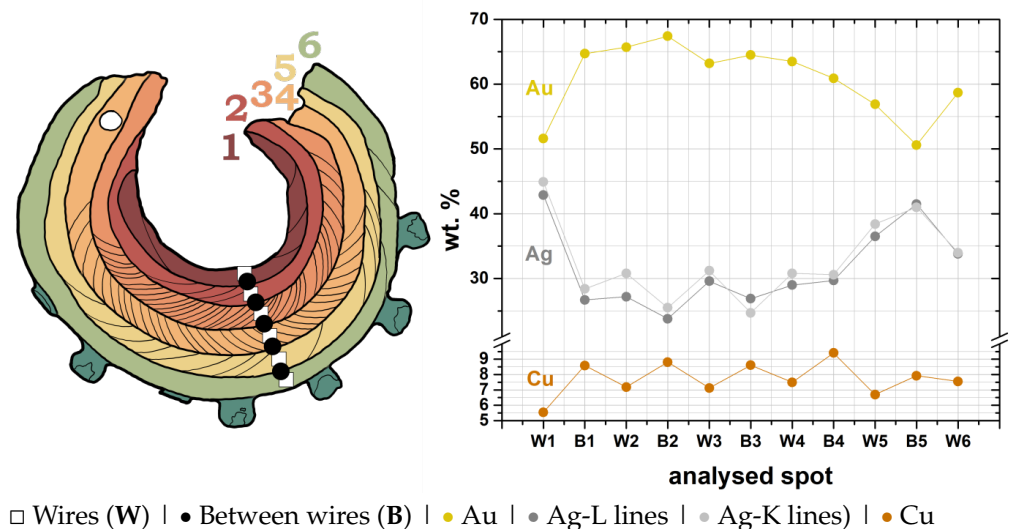
Figure 7. Micro-XRF analysis of the six wires (1 to 6) and the area between the wires of the earring, showing that there is a higher content of Au and Cu between the wires.
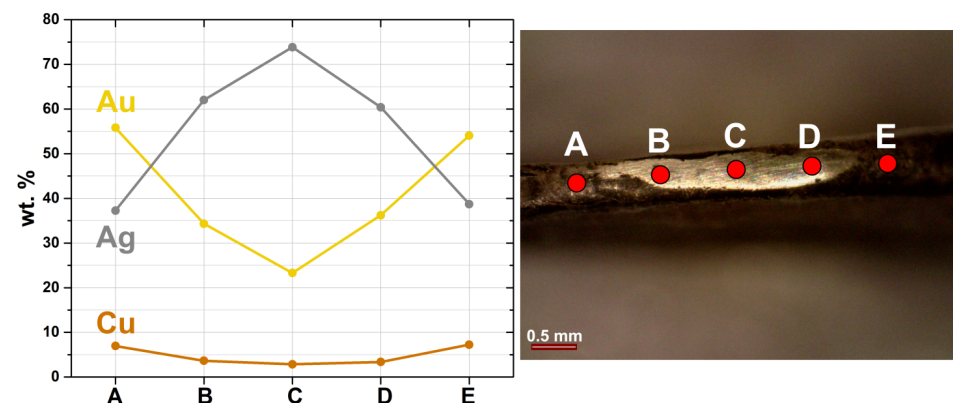
Figure 8. Micro-XRF analyses of the prepared area (1), showing a compositional gradient from the surface of the earring towards the centre of the prepared area (5 spot analyses, using Ag-K lines).

Figure 9. Micro-XRF results showing a compositional gradient from the surface of the earring towards the centre of the prepared area (1) (Ag-K lines used). Results show a positive correlation between the Au and Cu contents.
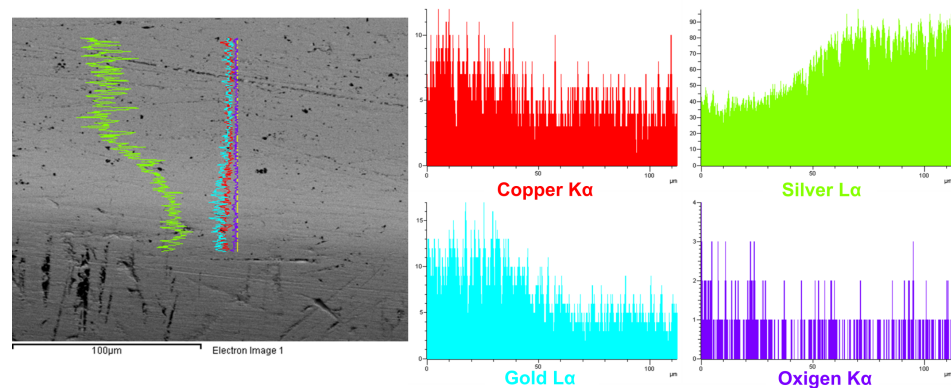
Figure 10. SEM-EDS analysis of the prepared area (1), with a (BSE) image at left and a line scan of Cu, Ag, Au and O elements. The Ag content is higher towards the centre of the prepared area, and Au and Cu contents are higher towards the surface of the earring.

The analysis of the prepared area (2), corresponding to the fracture of a missing granule, can be interpreted as a cross-section in the region where the granule was fixed to the wire of the body-earring (Figure 11). Thus, besides representing a cross-section of the gold-rich coating it also provides information about the joining system of the silver granule to the wire. This area was analysed by SEM-EDS, and in a BSE image (Figure 12) it is possible to observe part of the granule now totally corroded (hollow) and a surrounding gold-rich layer that shows some composition heterogeneities. Near to the surface, the gold layer has several pores or oxides (small dots that ouline to the right side in the red area in Figure 12), 29–89 μm distant from the surface outline. EDS area analyses of this outer layer show an alloy composition of ~59 wt.% Au, 34 wt.% Ag and 8 wt.% Cu (Figure 12, area 1). In middle regions (areas 2 and 3), the composition of the alloy is very similar to area 1 (~60 wt.% Au, 32 wt.% Ag and 8 wt.% Cu). Only on the most internal area (4), the content of Ag increases significantly (~11 wt.% Au, 87 wt.% Ag and 2 wt.% Cu), with a composition that would probably be closer to the original silver granule composition.

Worth of notice is that the composition obtained for the outer layer is similar to the composition obtained in the micro-XRF analyses made in the areas between the wires,

and thus probably represents the nowadays composition of the gilding layer (Table 4). This composition is not the original composition of the gold alloy. If a hot bonding technique was used the original composition of the gold alloy was altered due to diffusion of metal from the gold layer into the silver base (and vice-versa). Nevertheless, it can be assured that the original gold alloy had much more Cu than nowadays analysed [39]. The thickness of this outer layer, with values between 29 to 89 μm, does also account for the same range of dimensions previously measured for the gold layer thickness by OM (Figure 4). This suggests that this outer layer (Figure 12, area 1) is the coating that entirely covers the object. The middle region (Figure 12, areas 2 and 3), which shows a similar composition to the outer layer, can be interpreted as being a solder that was used to join the silver granules to the silver wire. Previous analysis to IA artefacts from western Iberia have detected solders with a Cu-richer composition (~8 wt.% Cu) than the gold-alloys which were being united [14].

**Table 4.** Range of compositions obtained by micro-XRF of the areas between the wires.

|	Au (wt.%)	Ag (wt.%)	Cu (wt.%)
Using Ag-K lines	61.50–66.50	24.70–29.30	8.82–9.72
Using Ag-L lines	61.90–67.40	23.80–28.80	8.29–9.71
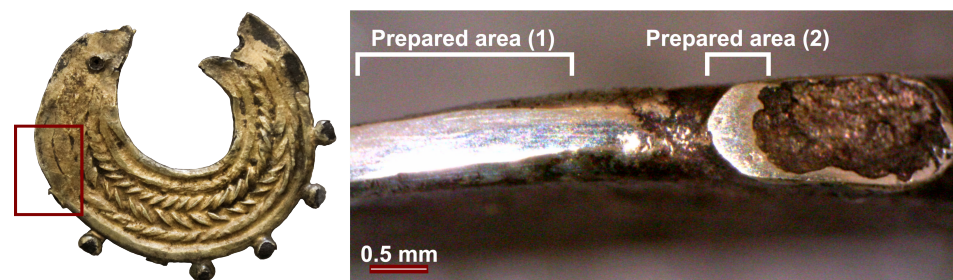
Figure 11. At the left the side region where surface preparation was performed in the earring is depicted. At right is an OM image of the prepared area (1) and (2).

Based on the SEM-EDS analysis made over the missing granule area (2), it can be proposed that the manufacturing of the earring included: (**a**) twisting and mechanically joining the six Ag wires at their tops; (**b**) joining the silver granules to the silver wire using an Au-Cu-rich solder (middle region in Figure 12); (**c**) gilding the entire earring using a similar Au-Cu-rich alloy as was used for the solder, ending up with a ~45 μm thick Au-rich layer all over the artefact (Figure 13). The precise gilding method is not known, but it certainly involved a diffusion bonding, being the circumference of pores detected in area (2) oxides or air bubbles that formed between the gold layer and the base metal during the gilding process of the artefact. The use of a gold alloy with a high amount of Cu could account for providing a lower *liquidus* temperature than pure gold so that it would lower the *liquidus* temperature to values closer/lower than the silver base metals.
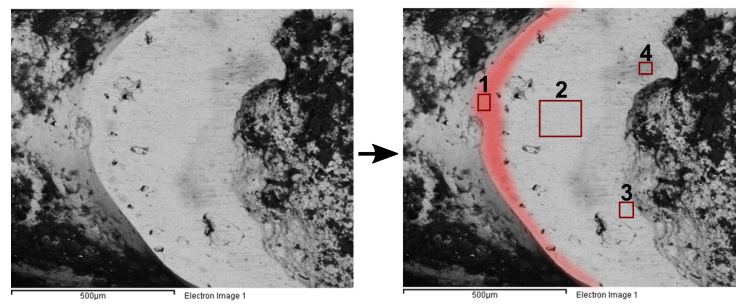
No. analysis	wt.%			Other elements
	Au	**Ag**	**Cu**	
1	58.78	33.68	7.54	C, O
2	60.28	31.39	8.32	O
3	58.87	34.53	6.60	O
4	11.35	86.96	1.69	O, Si

Figure 12. SEM-EDS analysis of the prepared area (2): on top (BSE) images with the gold layer highlighted in red and four areas analysed depicted; on bottom EDS results of the four analysed areas: (1) outer layer; (2, 3) middle region; (4) internal zone.

(a)

(b)

(c)
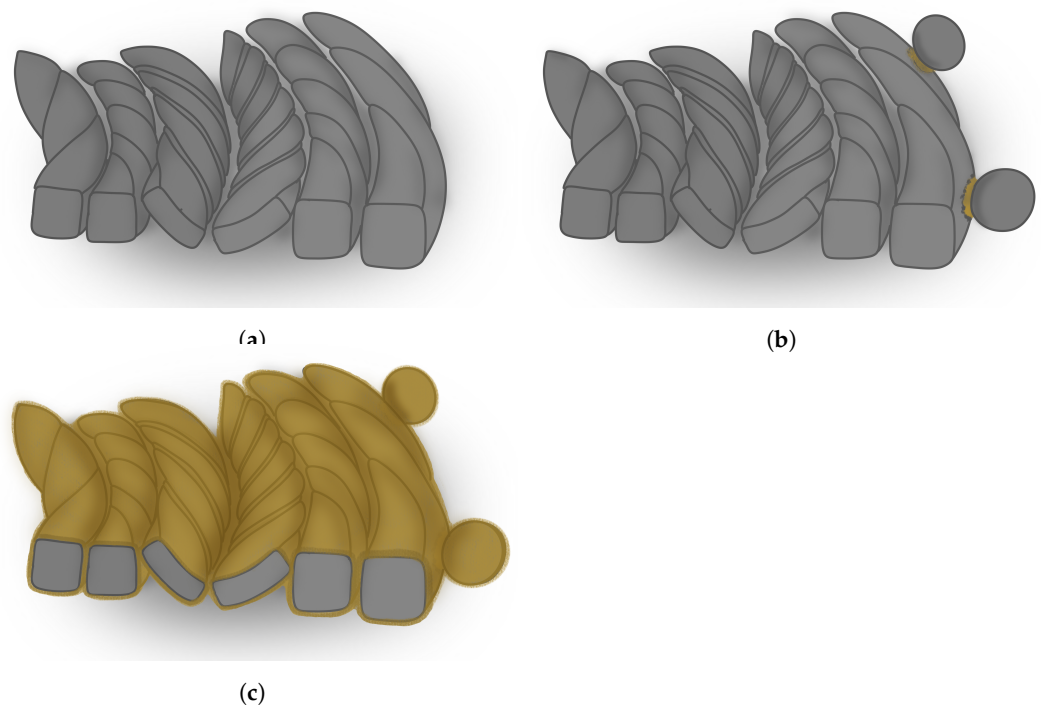
Figure 13. Scheme of a cross-section of the earring showing a proposal for the manufacturing sequence of the earing: (**a**) six twisted wires made of a Ag alloy; (**b**) joining the silver granules to the external silver wire using an Au-Cu-rich solder alloy; (**c**) gilding of the entire object with an Au-Cu-rich alloy of similar composition to the alloy used in (**b**).

4. Conclusions

The present work focused on the compositional and technological study of an earring from western Iberia attributed to the Iron Age. This artefact incorporates diverse metallurgical techniques, which include the fabrication of silver wires through torsion, the use of granules for aesthetic purposes, and the gilding of the entire object.

The wires that compose the body of the earring were twisted with the block- and strip-twist techniques, producing an elaborated visual effect. Both Z- and S-torsion were applied. The original composition of the wires was not fully determined but can be proposed as >74 wt.% Ag, <23 wt.% Au and <3 wt.% Cu. The silver granules that make the outline of the earring were also manufactured in a silver-rich alloy, whose original composition can be proposed as >87 wt.% Ag, <11 wt.% Au and <2 wt.% Cu. Possibly the wires and the granules were manufactured from the same alloy composition.

The gilding of the earring was made in a gold-rich alloy, with higher Cu content when compared to the silver alloy used for the wires and granules. The present measured composition of this layer was determined as ~60 wt.% Au, ~32 wt.% Ag and ~8 wt.% Cu. The same gold-rich alloy was probably also used to join the silver granules to the body of the artefact, prior to the final gilding. It was determined that the gold layer varies in thickness, reaching thicker values in areas between the wires. Yet, an average of 45 μm of thickness was measured on most areas. Adherence between the gold coating and the base metal was found to be strong, and the analysis of the prepared area (2) determined that the gilding process most likely involved a diffusion process. Consequently, the original composition of the gold alloy cannot be totally determined, i.e., the measured Ag content can result from the diffusion of the base silver metal during the gilding process. This gold coating was probably applied to confer a greater value to the object, being that silver that was used for the metal core would bear a smaller economic and/or aesthetic value than gold.

The present study, involving complementary examination and analytical techniques such as digital optical microscopy observations, XRF analysis using Ag-K lines and Ag-L lines, and SEM-EDS analysis, was very important to allow the identification of a gilded artefact. To our knowledge, this is the first Iron Age gilded silver earring identified in western Iberia. This approach may lead to the future identification of other gilded earrings, using a minimally invasive analytical approach.

Finally, the identification of gilded artefacts is also important for the establishment of future conservation approaches, since Au-rich and Au-rich alloys show very different susceptibilities to corrosion.

Abbreviations

The following abbreviations are used in this manuscript:

BA	Bronze Age
BCE	before common era
BSE	backscattered electrons
EDOF	extended depth of field
IA	Iron Age
LBA	Late Bronze Age
LIA	Late Iron Age
micro-XRF	micro X-ray fluorescence spectrometry
OM	optical microscope
pXRF	portable X-ray fluorescence spectrometry
SE	secondary electrons
SEM-EDS	scanning electron microscopy with energy dispersive spectroscopy
SM	snap mode

References

1. Armada, X.L.; García-Vuelta, Ó. Plano-convex ingots and precious metalwork in northwestern Iberia during the Late Iron Age and Early Roman period: An analytical approach. *Archaeol. Anthropol. Sci.* **2021**, *78*, 1–22. [CrossRef]
2. Armbruster, B.; Parreira, R. *Inventário do Museu Nacional de Arqueologia: Coleção de Ourivesaria – do Calcolítico à Idade do Bronze*, 1st ed.; Secretaria de Estado da Cultura: Lisbon, Portugal, 1993; Volume 1, pp. 17–32.
3. Cardoso, M. Das origens e técnica do trabalho do ouro e sua relação com a joalharia arcaica peninsular. *Rev. De Guimarães* **1957**, *67*, 5–46.
4. Perea, A. *Orfebrería Prerromana: Arqueologia del Oro*, 1st ed.; Caja de Madrid: Madrid, Spain, 1991.
5. Armbruster, B. *Les ors de l'Europe Atlantique à l'âge du Bronze—Technologie et Ateliers*; Association des Publications Chauvinoises (A.P.C.): Chauvigny, France, 2021.
6. Guerra, M.F.; Tissot, I. Analytical study of Bronze Age goldwork from Northwest Iberia. *J. Archaeol. Sci. Rep.* **2021**, *39*, 103–117. [CrossRef]
7. Guerra, M.F.; Tissot, I. The role of nuclear microprobes in the study of technology, provenance and corrosion of cultural heritage: The case of gold and silver items. *Nucl. Instruments Methods Phys. Res. Sect. B Beam Interact. Mater. Atoms* **2013**, *306*, 227–321. [CrossRef]
8. Armbruster, B.; Perea, A. Macizo/Hueco, Soldado/Fundido, Morfología/ Tecnología. El ámbito Tecnológico Castreño a través de los torques con remates en doble escocia. *Trab. Prehist.* **2000**, *57*, 97–114. [CrossRef]
9. Perea, A.; García-Vuelta, Ó. Gold usage: Wear marks and/or deterioration in site conditions. In *Historical Technology, Materials and Conservation: SEM and Microanalysis*; Archetype Books: London, UK, 2012; pp. 86–92.
10. Allan, G.; Woodcock, J. A review of the flotation of native gold and electrum. *Miner. Eng.* **2001**, *14*, 931–962. [CrossRef]
11. Montero, I.; Rovira, S. El Oro y sus aleaciones en la Orfebrería Prerromana. *Arch. EspañOl Arqueol.* **1991**, *64*, 163–164. [CrossRef]
12. Armada, X.L.; García-Vuelta, Ó. Iron Age gold in Northwestern Iberia: Technology, chronology, and social meaning. In *Early Iron Age Gold in Celtic Europe: Society, Technology and Archaeometry*; Verlag Marie Leidorf GmbH: Toulouse, France, 2018; pp. 321–338.
13. Loureiro, J.; Figueiredo, E.; Silva, R.J.C.; Araújo, M.F.; Fonte, J.; Bettencourt, A.M.S. Metal alloys, matrix inclusions and manufacturing techniques of Moinhos de Golas collection (North Portugal): A study by micro-EDXRF, SEM-EDS, optical microscopy and X-Ray radiography. *Appl. Phys. A* **2016**, *122*, 1–12. [CrossRef]
14. Valério, P.; Silva, R.J.C.; Monge Soares, A.M.; Araújo, M.F.; Baptista, L.; Calvo, E. Microanalytical Study of Ancient Gold Jewelry: Mediterranean Impact on the Early Iron Age Technology in Southwestern Iberia. *Microsc. Microanal.* **2019**, *25*, 1061–1073. [CrossRef]
15. Virgílio, H.C.; Parreira, R.; Silva, A.C.F. *Ourivesaria Arcaica em Portugal: O Brilho do Poder*; CTT: Lisbon, Portugal, 2013.
16. Figueiredo, E.; Silva, R.J.C.; Araújo, M.F.; Senna-Martinez, J.C. Identification of ancient gilding technology and Late Bronze Age metallurgy by EDXRF, Micro-EDXRF, SEM-EDS and metallographic techniques. *Microchim. Acta* **2010**, *168*, 283–291. [CrossRef]
17. Martinón-Torres, M.; Ladra, L. A Ourivería prehistórica no Museo Provincial de Lugo: Unha aproximación desde a química. In *A Colección de Ourivería Antiga do Museo Provincial de Lugo*, 1st ed.; García, A., Ed.; Servizo de Publicacións da Deputación de Lugo: Lugo, Spain, 2018; pp. 46–59.
18. Monge Soares, A.M.; Valério, P.; Silva, R.J.C.; Alves, L.; Araújo, M.F. Early Iron Age gold buttons from Southwestern Iberian Peninsula, identification of a gold metallurgical workshop. *Trab. Prehist.* **2010**, *67*, 501–510. [CrossRef]
19. Guerra, M.F.; Tissot, I. Bronze Age and Iron Age gold torcs and earrings from the Iberian Atlantic façade: A non-invasive multi-analytical approach to the characterisation of the alloys and the corrosion. *X-Ray Spectrom.* **2015**, *45*, 5–13. [CrossRef]
20. García-Vuelta, Ó.; Montero Ruiz, I.; Villa Valdés, Á. Orfebrería Castreña en el Museo Arqueológico de Asturias (Oviedo): Aproximación a su caracterización arqueométrica y problemas de estúdio. *Trab. Prehist.* **2020**, *77*, 163–183. [CrossRef]
21. Armada, X.L.; García-Vuelta, Ó.; Kaal, J.; Martín-Seijo, M.; Porto, Y. Characterization of cores and organic remains in Iron Age gold objects: The Recouso treasure. *Mater. Manuf. Process.* **2017**, *32*, 740–748. [CrossRef]

22. Mello, E.; Parrini, P.; Formigli, E. Etruscan filigree: Welding techniques of two gold bracelets from Vetulonia. *Am. J. Archaeol.* **1983**, *87*, 548–551. [CrossRef]
23. Effenberg, G.; Ilyenko, S. *Noble Metal Systems: Selected systems from Ag-Al-Zn to Rh-Ru-Sc*; Springer: Heidelberg, Berlin, Germany, 2006; p. 10.
24. Guerra, M.F.; Tissot, I. *A Ourivesaria Pré-Histórica do Ocidente Peninsular Atlântico: Compreender Para Preservar*; Guerra, M.F., Tissot, I., Eds.; Projeto AuCORRE; Louresgráfica: Loures, Portugal, 2013.
25. Vitobello, M.L.; Rehren, T.; Vitobello, M.L.; Rehren, T.*A quest for authenticity*;Institute of Archaeology: London, UK, 2009.
26. Ogden, J. Classical gold wire: Some aspects of its manufacture and use. *Jewel. Stud.* **1991**, *5*, 95–105.
27. García Castro, J.A. *El Oro en la España Prerromana: Arqueologia del Oro*; Caja de Madrid: Madrid, Spain, 1989.
28. Taylor, J. *Bronze Age Goldwork of the British Isles*; Cambridge University Press: Cambridge, UK, 1980.
29. Scott, D.A. The deterioration of gold alloys and some aspects of their conservation. *Stud. Conserv.* **1983**, *28*, 194–203.
30. Figueiredo, E.; Silva, R.J.C.; Araújo, M.F.; Fernandes, F.M.B. Multifocus Optical Microscopy Applied to the Study of Archaeological Metals. *Microsc. Microanal.* **2013**, *19*, 1248–1254. [CrossRef]
31. McKerrell, H. Non-dispersive XRF applied to ancient metalworking in copper and tin bronze. In *X-ray Microfluorescence Analysis Applied to Archaeology, Proceedings of the Symposium PACT 1, Conseil de l'Europe*; García, A., Ed.; Assemblée parlementaire: Strasbourg, France, 1977; pp. 138–173.
32. Cowell, M. Energy dispersive X-ray fluorescence analysis of ancient gold alloys. In *X-ray Microfluorescence Analysis Applied to Archaeology, Proceedings of the Symposium PACT 1, Conseil de l'Europe*; García, A., Ed.; Assemblée parlementaire: Strasbourg, France, 1977; pp. 76–85.
33. Bandyopadhyay, P.; Segre, C.U. Mucal on the Web. Available online: http://www.csrri.iit.edu/mucal.html (accessed on 17 January 2023).
34. Goldstein, J.; Newbury, D.; Echlin, P.; Joy, D.; Lyman, C.; Lifshin, E.; Sawyer, L.; Michael, J. *Scanning Electron Microscopy and X-Ray Microanalysis*, 3rd ed.; Kluwer Academic/Plenum Publishers: New York, NY, USA; Boston, MA, USA; Dordrecht, The Netherlands ; Longon, UK; Moscow, Russia, 2003.
35. Lins, P.A.; Oddy, W.A. The Origins of Mercury Gilding. *J. Archaeol. Sci.* **1975**, *2*, 365–373. [CrossRef]
36. Perea, A.; Montero, I.; Gutiérrez, P.C.; Climent-Font, A. Origen y trayectoria de una técnica esquiva: El dorado sobre metal. *Trab. Prehist.* **2008**, *65*, 117–130.
37. Martinón-Torres, M.; Ladra, L. Orígenes del dorado por amalgama: Aportaciones desde la orfebrería protohistórica del noroeste de la Península Ibérica. *Trab. Prehist.* **2011**, *68*, 187–198. [CrossRef]
38. Valério, P.; Monge Soares, A.M.; Silva, R.J.C.; Araújo, M.F.; Rebelo, P.; Neto, N.; Santos, R.; Fontes, T. Bronze production in Southwestern Iberian Peninsula: The Late Bronze Age metallurgical workshop from Entre Águas 5 (Portugal). *J. Archaeol. Sci.* **2013**, *40*, 439–451. [CrossRef]
39. Scrivano, S.; Gómez-Tubío, B.; Ortega-Feliu, I.; Ager, F.J.; Moreno-Suárez, A.I.; Respaldiza, M.A.; de la Bandera, M.L.; Marmolejo, A. Identification of soldering and welding processes in ancient gold jewelry by micro-XRF spectroscopy. *X-ray Spectrom.* **2013**, *42*, 251–255. [CrossRef]